

FE Simulations of Irreversible Relative Movements (Creeping) in Rolling Bearing Seats - Influential Parameters and Remedies

A. Maiwald, E. Leidich

Abstract— The effect of irreversible relative movements, i.e., creeping, in rolling bearing seats is a highly topical issue. Creeping leads to a continuous rotation of the bearing ring relative to the connection geometry (housing or shaft). It may cause wear in the bearing seats, followed by bearing failure. Therefore, creeping must absolutely be avoided. This study focused on the influence factors that cause creeping phenomena. Additionally, methods to reduce the creeping effects were defined. Finally, an algorithm for the analytical determination of the critical creeping load was developed. This work enables the user to develop concrete information to optimize a bearing with respect to the bearing seat design and the selection of the roller bearing to prevent creep damage.

Index Terms— roller bearing, bearing seat, creeping, FE simulations

I. INTRODUCTION

ROLLER bearings are used in many important applications. With respect to bearing design, the bearing seats are the primary focus. Issues develop in the bearing seats with increasing performance and higher dynamic stresses, which can lead to irreversible relative movements, i.e., creeping, between the bearing rings and the shaft or the housing. These relative movements are accompanied by the formation of corrosion in the bearing seat, which can lead to fractures of the shaft at the seat of the inner ring. Creeping can also result in wear, which can cause shaft displacements with serious consequences, e.g., for the tooth meshing in the gearbox. Various insurance companies describe the creeping of bearing rings (races) as the main damage focus in gearboxes in wind turbines. The follow-up costs for the operator, and ultimately for the manufacturer, are usually considerable. The topic is highly relevant, as there is a requirement for the growth of renewable energy sources, and wind power is an important source of renewable energy [1]–[4]. In this paper, a complex kinematic 3D finite element (FE) multi-body simulation of a rolling bearing is presented. Using this simulation method, a detailed analysis of the creeping of the bearing ring (race) is

Manuscript received April 26, 2013; revised May 08, 2013. The authors would like to thank the German organizations Forschungsvereinigung Antriebstechnik e.V. (FVA), Bundesministerium für Wirtschaft und Technologie (BMWi) and Arbeitsgemeinschaft industrieller Forschungsvereinigungen "Otto von Guericke" e.V. (AiF) for the financial support of the projects FVA 479 I and IGF-Nr. 15652 BG.

A. Maiwald and E. Leidich are with the Department of Engineering Design, Chemnitz University of Technology, 09126 Chemnitz, Germany (e-mail: andreas.maiwald@mb.tu-chemnitz.de)

presented for the first time, which introduces new opportunities to research in creeping processes. Furthermore, this method replaces complex and expensive

experiments on the original bearing. The focus of these studies is on the outer rings of the radial bearings under a point load. Outer rings are typically provided with a clearance fit and are thus more prone to creeping than are bearing seats with an interference fit.

II. CREEPING

Creeping describes flexing micro-movements of the bearing ring relative to the connection geometry. In contrast to tangential slip in shaft-hub connections, these movements occur without nominal torsional loading. In Fig. 1, a simplified diagram of the creeping process is shown. As shown in the diagram, even a pure normal load (bearing rests) leads to a wave-like deformation of the bearing ring, which is shown as a plate. The rotation of the bearing creates a combined load of normal and tangential forces on the bearing ring. This combined load generates a slip wave in the bearing seat, which leads to a continuous shift, Δ , between the contacting surfaces.

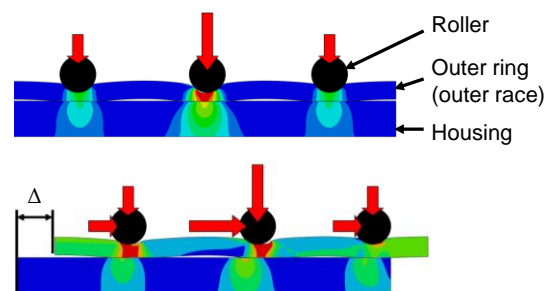


Fig. 1. Simplified representation of creeping movement at the plate. Normal load (above) and combined normal and tangential load (below).

III. FE KINEMATIC SIMULATION TO INVESTIGATE CREEPING

A. Model structure

In the following, the computational implementation of the kinematic simulation is briefly explained. Fig. 2 shows the 3D model of the bearing NU 205, which is simulated using approximately 120,000 elements. To simplify the model structure without significant loss of precision, only the outer ring, with the rolling elements, and the housing are modeled. The housing and the outer ring are modeled as independent elastic solids. The rolling elements are rigid bodies. They are coupled by a prismatic joint with a central reference

point (Fig. 3). Thus, each rolling element has only one degree of freedom in the radial direction. This radial degree of freedom is eliminated by the loads of the rolling elements, which can be calculated according to DIN ISO 281 [5]. By rotation of the reference point, the rolling elements move circumferentially and slide frictionless over the contact surface of the outer ring. For all simulations (unless otherwise specified) the coefficient of friction in the bearing seat is set to $\mu = 0.3$. This value corresponds to oil-lubricated steel-steel contact (100Cr6 E vs. 42CrMo4 +QT) after the “running-in phase”, and has been determined experimentally in [3].

A detailed description of the complete simulation methodology can be found in [4]. For the FE analysis, version 6.10-3 of the ABAQUS software was used.

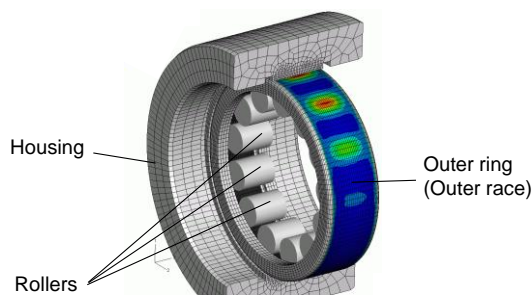


Fig. 2. Model of the simulated bearing NU 205.

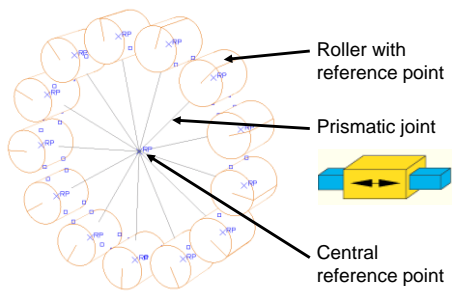


Fig. 3. Substitution of the cage.

B. Analysis of creeping data

The creeping torque, T_C , is evaluated to measure the intensity of creeping in the simulated bearing ring. This parameter describes the torque in the circumferential direction, which is needed to prevent the macroscopic relative movement (creeping) between the housing and the bearing ring (Fig. 4). A high creeping torque corresponds to a large creeping intensity of the bearing ring and is therefore classified as negative and converse.

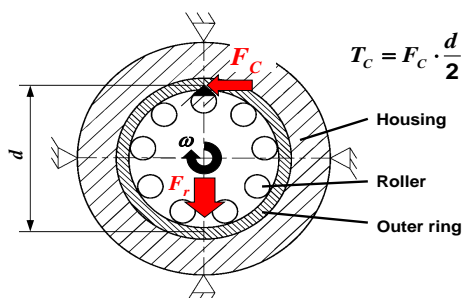


Fig. 4. Model for the determination of the creeping force, F_C , with respect to the creeping torque, T_C .

C. Reference geometry

Fig. 5 shows all geometric parameters for the simulation results presented below.

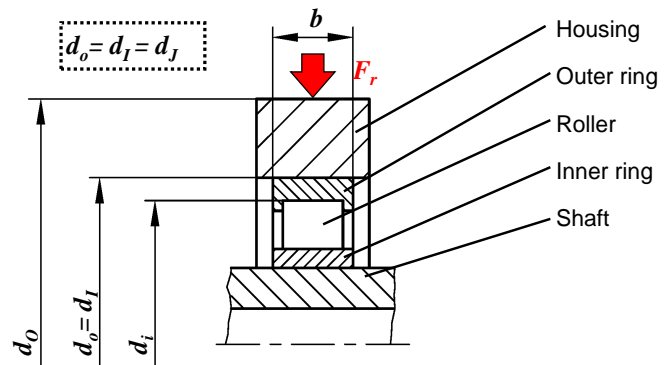


Fig. 5. Geometric parameters and definition of joint diameter, d_j .

The thickness ratio, Q , of the inner and the outer diameter is used to describe the wall thickness of the cylindrical components as follows:

$$Q_b = \frac{d_i}{d_o}, \quad Q_h = \frac{d_I}{d_o} \quad (1)$$

To characterize the interference, or clearance fit, it is normalized by the joint diameter, d_j . By definition, the normalized clearance fit, ζ^* , has negative values and is expressed as follows:

$$\zeta \triangleq \zeta^* = \frac{\Delta d}{d_j} \quad (2)$$

The bearing load is divided by the projected surface area of the bearing seat, A_{proj} . This results in the surface area-normalized radial load, p_r , as follows:

$$p_r = \frac{F_r}{A_{proj}}, \quad \text{where } A_{proj} = b \cdot d_o, \quad (3)$$

which is analogous to the bearing stress.

IV. VALIDATION OF THE FE-KINEMATIC SIMULATION

Using the current FE model, creeping movements are realistically simulated with the aid of FEM for the first time. The simulation results correlate with the experimental data [3]–[6]. This is demonstrated by the comparison of experimental and simulated results shown in Fig. 6. Thus, the simulation enables the user to perform extensive parameter variations to investigate the effects of creeping, which were not previously possible. Thus, the use of cost-intensive experiments is no longer necessary.

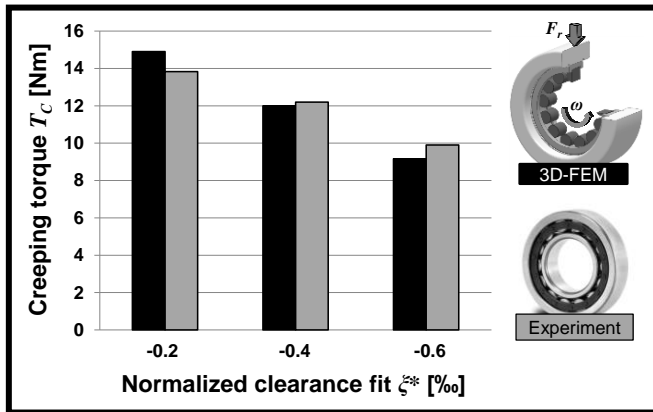


Fig. 6. Comparison of the creeping torque between 3D FE simulation and experiment for the example of the normalized clearance fit, ζ^* , between the housing and the outer ring. (Reference data: Bearing NU 205; normalized radial load, $p_r = 18$ MPa; coefficient of friction between the outer ring and housing, $\mu = 0.3$; elastic modulus of the housing, $E = 210$ GPa)

V. PARAMETER ANALYSIS OF THE CREEPING BEHAVIOR OF ROLLER BEARINGS FOR THE EXAMPLE OF THE OUTER RING OF THE CYLINDRICAL ROLLER BEARING NU 205

A. Influence of the bearing housing

In Fig. 7, the influence of the bearing housing on the creeping behavior by changing the modulus of elasticity, E , the thickness ratio, Q_h with respect to the housing stiffness and the coefficient of friction between the outer ring and the housing μ is illustrated.

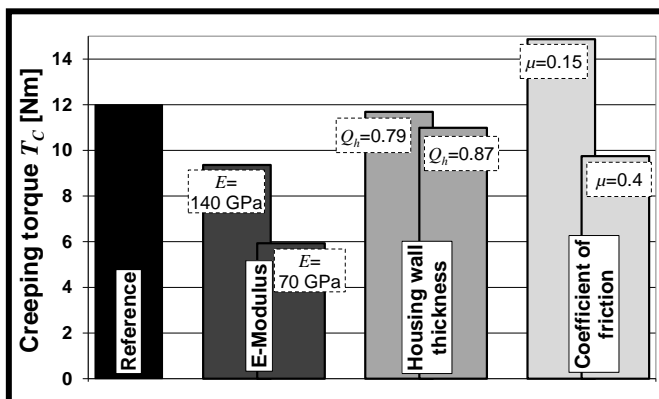


Fig. 7. Change of the creeping torque from variations in the modulus of elasticity of the housing, E , the housing wall thickness, Q_h and the coefficient of friction between the outer ring and the housing, μ . (Reference data: Bearing NU 205; normalized radial load, $p_r = 18$ MPa; $\mu = 0.3$; normalized clearance fit, $\zeta^* = -0.4$ %; $E = 210$ GPa; $Q_h = 0.69$)

The results show that with a decreasing modulus of elasticity, E , the creeping torque, T_c , decreases also. This is because a softer housing is better able to absorb the creeping motion of the bearing ring (Fig. 8). Thus, the bearing seat area between two loaded rolling elements (see Fig. 1) is exposed to a local contact pressure increase. Therefore, in this creeping-critical bearing seat area (see Chapter 2), higher local contact shear stresses are transferable, which leads to a reduction or prevention of creeping of the bearing ring. Through the implementation of elastic thin-walled housing structures (lower housing wall thickness), the torque is only marginally reduced. The influence of the modulus of elasticity, in contrast to the housing wall thickness, is much higher.

As expected, a higher coefficient of friction in the bearing seat leads to a reduction of the creeping torque. Therefore, arrangements to increase the coefficient of friction (surface coating, etc.) are recommended. Possible solutions are presented in [7].

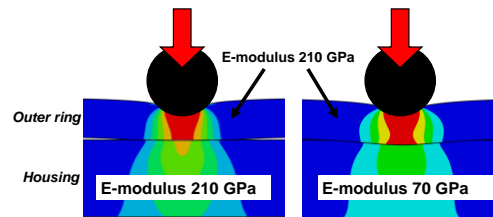


Fig. 8. Qualitative representation of the absorption of the bearing ring deformation under normal load conditions by varying the housing stiffness through the modulus of elasticity, E .

B. Influence of the bearing parameters

Fig. 9 shows the influence of the bearing parameters on the creeping behavior by comparing the results with different thickness ratios of the outer ring, Q_b , numbers of rollers, Z , and surface area-normalized radial loads, p_r .

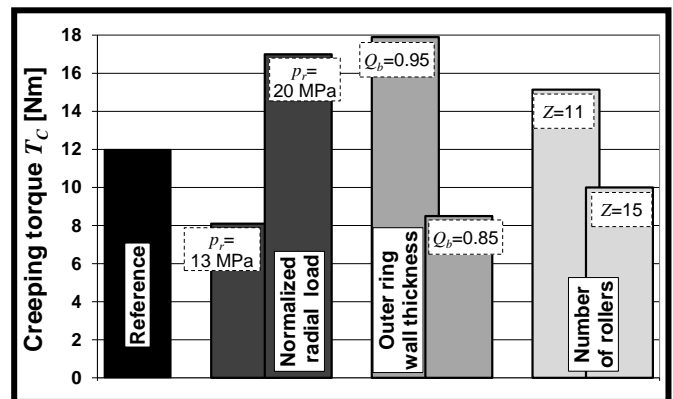


Fig. 9. Change of the creeping torque with variations of the thickness ratio of the outer ring, Q_b , the number of rollers, Z , and the surface area-normalized radial load, p_r . (Reference data: Bearing NU 205; $p_r = 18$ MPa; coefficient of friction in the bearing seat, $\mu = 0.3$; normalized clearance fit, $\zeta^* = -0.4$ %; modulus of elasticity of the housing, $E = 210$ GPa; $Z = 13$; $Q_b = 0.90$)

The results show that thick bearing rings ($Q_b = 0.85$) have less inclination to creep than thin because of the increased stiffness of thick-walled bearing rings. The thick-walled bearing ring deforms less (see Chapter 2), and the creeping process is inhibited.

In addition, reduction of the radial load leads to a decrease in the creeping torque. This relation is based on the fundamental processes of creeping, i.e., creeping occurs primarily from the formation of slip in the bearing seat as a result of the tangential deformation of the loaded bearing ring (see Chapter 2). If the load is small, the tangential deformation and, thus, the creeping torque are also small. Fig. 9 also shows that the increase in the number of rollers, with an identical bearing load, results in a decreased creeping torque. This is because of reduced roller loads, which reduces the tangential deformation of the bearing ring.

C. Influence of the fit

In Fig. 10 the effect of the normalized interference fit, ζ , and clearance fit, ζ^* , between housing and outer ring on the creeping behavior is shown. The results show that an increase of the normalized clearance fit, $\zeta^* = -0.1\%$ to -0.6% results in a reduction of the creeping torque.

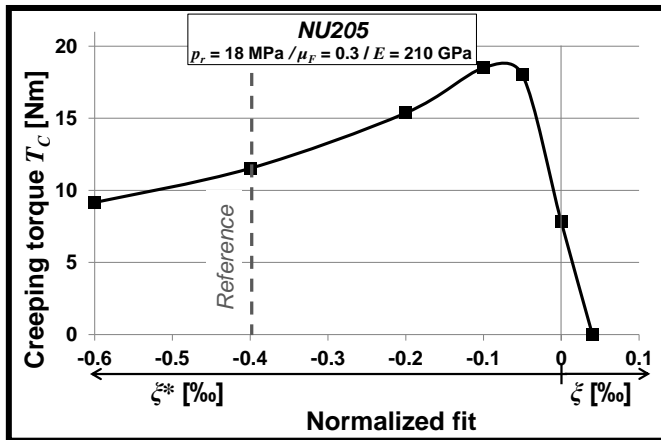


Fig. 10. Change of the creeping torque from a variation of the normalized clearance fit ($\zeta^* < 0$) and the normalized interference fit ($\zeta \geq 0$) between the housing and the outer ring.

In [3] and [6], this creeping behavior is verified experimentally. The effect of the clearance fit can be explained by the modification of the load zone (Fig. 11). Increasing the clearance fit (and/or the bearing clearance) leads to a reduction of the load zone, i.e., fewer rollers are used to transfer the bearing load. The load transfer is thus based on a smaller contact surface area and a higher contact pressure, thus increasing the transferable local contact shear stress. The reduction in stress leads to a reduction in or the prevention of creeping.

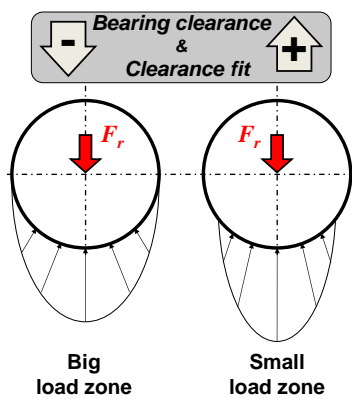


Fig. 11. Different load zones in reliance to the clearance fit.

D. Other important parameters

In addition to the parameter analysis presented, other influences on creeping were determined in [4] and [8]. Those studies developed recommendations for bearing seat design. An overview of those solutions is shown in Fig. 12.

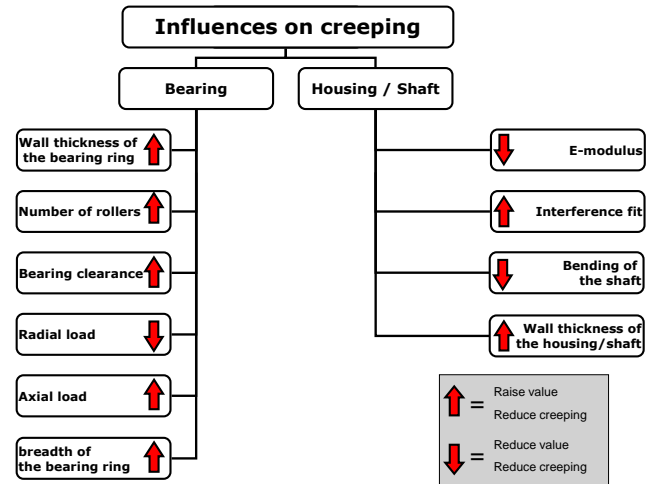


Fig. 12. Effects of relevant bearing parameters on creeping [4].

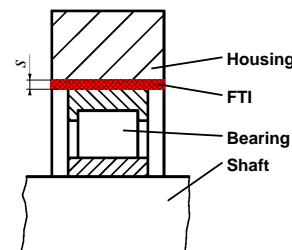
VI. ADDITIONAL CONSTRUCTIVE CAPABILITIES TO REDUCE CREEPING

A. Flexible thin-film interlayer (FTI)

As a possible remedy against walking (based on the results presented in Chapter 4, i.e., that the creeping moment decreases by a reduction in the modulus of elasticity), a flexible thin-film interlayer (FTI) between the housing and the bearing ring was simulated (Fig. 13). The housing is made of a partitioned continuum representing the two material areas of FTI and regular housing material. Thus, the contact surfaces between FTI and housing are neglected, which would correspond to bonding of the contact materials.

The simulation results presented in Fig. 14 show that as the modulus of elasticity of the FTI decreases, the creeping torque also decreases. With the use of polyamide, the reduction can be as large as 40%. The opposite trend for the polyamide-FTI with the larger wall thickness, $s = 300 \mu\text{m}$ (compared to $s = 200 \mu\text{m}$), is due to the reduced tangential stiffness for the thicker FTI. The polyamide is strongly deformed by the operating loads, and as a result of the model structure (locking of the outer ring in the circumferential direction, cf. Fig. 4), the creeping torque increases.

The simulation of magnesium as the FTI material shows the limitations of the FTI, achieving only a marginal reduction of the creeping torque.



Material	E-Modulus of the FTI E_{FTI} [GPa]
Magnesium	42
Polyamide	4

Fig. 13. Schematic diagram of the FTI (left) and the material characteristics of the FTI (right).

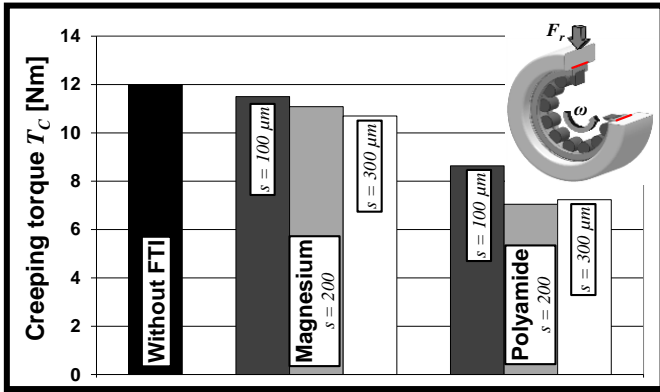


Fig. 14. Comparison of the creeping torque for varying wall thickness, s , and material properties of the FTL. (Reference data: Bearing NU 205; normalized radial load, $p_r = 18$ MPa; coefficient of friction in the bearing seat, $\mu = 0.3$; normalized clearance fit, $\xi^* = -0.4$ ‰; modulus of elasticity of the housing, $E = 210$ GPa)

B. Form-fitted creeping lock

For heavily loaded bearings and critical creeping applications, a form-fitted connection between the bearing ring and the housing, including the shaft, is essential. Fig. 15 shows the circumferential forces between the outer ring and the housing, which must be absorbed by a form-fitted creeping lock. It were researched a rigid element (the reference) and two elastic spring elements. Each spring element can be described by a linear spring characteristic curve, which is defined by a spring rate, $c = F_w/\Delta l$. The spring deflection, Δl , is thus equivalent to the relative movement between the housing and the outer ring (global slip). The results show that a soft form-fitted creeping lock has to take substantially lower loads than a rigid one. Further studies on the subject are part of the ongoing German research project Abhilfemaßnahmen Wandern (remedies for creeping) [9].

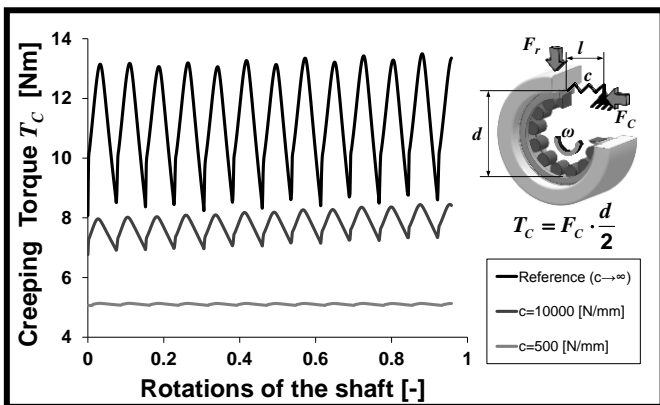


Fig. 15. Creeping torque as a function of the elasticity of the form-fitted creeping lock between the outer ring and the housing. (Reference data: Bearing NU 205; normalized radial load, $p_r = 18$ MPa; coefficient of friction in the bearing seat, $\mu = 0.3$; normalized clearance fit, $\xi^* = -0.4$ ‰; modulus of elasticity of the housing, $E = 210$ GPa)

VII. CALCULATION METHODS TO DETERMINE THE CRITICAL CREEPING LOAD

A fundamental goal for the practical implementation of the results is the development and verification of a calculation model to determine the critical creeping load of a bearing. The model should provide a rough estimate of the

bearing load when approaching the onset of creeping. Implementation of this model can thus limit the usage of complex, computationally intensive 3D FE simulations in bearing design. The following algorithm is used to calculate the critical creeping load for the outer ring of roller bearings under radial loads. It states that creeping starts when a load-induced slip zone extends over the entire width of the bearing ring. Unfortunately, slip cannot be calculated using analytical equations. Therefore, the calculation of the inception of slip is done with the radial stress ($\sigma_{rr}(F_i, \varphi)$) and shear stress ($\tau(F_i, \varphi)$) acting on the bearing seat as follows (Eqs. 4 and 5 from [10]):

$$\sigma_{rr}(F_i, \varphi) = \frac{F_i}{\pi \cdot b} \left[\frac{2 \cdot (D \cdot \cos \varphi - r) \cdot \left[\frac{(r^2 + D^2) \cdot \cos \varphi - D \cdot r \cdot (1 + (\cos \varphi)^2)}{r^2 + D^2 - 2 \cdot D \cdot r \cdot \cos \varphi} \right]}{r^2 + D^2 - 2 \cdot D \cdot r \cdot \cos \varphi} \right] \quad (4)$$

$$\tau(F_i, \varphi) = \frac{F_i}{\pi \cdot b} \left[\frac{2 \cdot D \cdot \sin \varphi \cdot (r - D \cdot \cos \varphi) \cdot (D - r \cdot \cos \varphi)}{r^2 + D^2 - 2 \cdot D \cdot r \cdot \cos \varphi} + \frac{5 - \nu}{4} \cdot \frac{\cos \varphi}{r} - D^2 \cdot \frac{3 - \nu \cos \varphi}{4 \cdot r^3} - \frac{D}{2 \cdot r^2} \right] \quad (5)$$

Based on Eqs. 4 and 5, the total stress from a single roller force is then added by angular transformation to the total stresses of the other individual roller forces (all forces together reflect the bearing load, as shown in Fig. 16) as follows:

$$\sigma(F_r, \varphi) = \sum \sigma(F_i, \varphi) \quad (6)$$

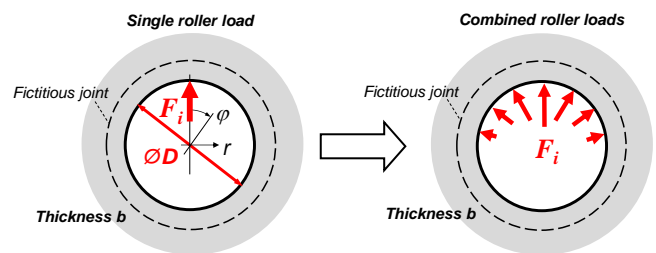


Fig. 16. Mechanical model (circular hole in an infinite plate) for the outer ring of a radially loaded bearing [4].

Finally, using the generalized Coulomb friction law, the transferable local shear stresses in the bearing seat, $\tau_{tr}(F_i, \varphi)$, are calculated as follows:

$$\tau_{tr}(F_r, \varphi) = \mu_F \cdot \sigma_{rr}(F_r, \varphi) \quad (7)$$

To ensure a creeping-safe bearing, the transferable local shear stresses, $\tau_{tr}(F_i, \varphi)$, must not be exceeded by the local shear stresses, $\tau(F_i, \varphi)$, over the complete circumference.

The safety against creeping, S_C , is also included in the calculation as follows:

$$\tau(F_r, \varphi) \leq \frac{\tau_{ir}(F_r, \varphi)}{S_C} \quad (8)$$

This calculation model, along with other algorithms (calculation of the inner ring and of the creeping torque), have been programmed by the German research association Forschungsvereinigung Antriebstechnik e.V. (FVA). As a result, the fully automated calculation tool, SimWag, is available, which enables the user to construct bearing seats without creeping.

VIII. SUMMARY

In this paper, numerical analyses of the creeping behavior of roller bearings are presented. With the aid of various complex 3D finite element kinematic simulations, the creeping mechanism is determined. Creeping describes flexing micro-movements (slip) of the loaded bearing ring. This slip leads to a substantial continuous rotation of the bearing ring relative to the connection geometry (housing or shaft). Through the studies performed, important influencing parameters are detected that cause or encourage creeping.

Furthermore, approaches for geometric and constructive remedies for reducing or eliminating creeping are discussed. Finally, an algorithm for the analytical determination of the creeping critical load of the outer ring is presented.

REFERENCES

- [1] Leidich, E.; Walter, V.; Maiwald, A.: Relativbewegungen von Wälzlageringern. Mainz: Vereinigte Fachverlage, Journal „Antriebstechnik“, Issue 11, 2009, pp. 70-76
- [2] Leidich, E.; Maiwald, A.; Gacka, A.: Wenig wandern, länger leben. Mainz: Vereinigte Fachverlage, Journal „Antriebstechnik“, Issue 06, 2012, pp. 18-21
- [3] Babbick, T.: Wandern von Wälzlageringern unter Punktlast. Doctoral thesis, TU Kaiserslautern, 2012
- [4] Leidich, E.; Sauer, B.; Maiwald, A.; Babbick, T.: Beanspruchungsgerechte Auslegung von Wälzlagersitzen unter Berücksichtigung von Schlupf- und Wandereffekten. Frankfurt/M.: Forschungsvereinigung Antriebstechnik e.V., Journal Nr. 956, 2010
- [5] DIN ISO 281, Wälzlager - Dynamische Tragzahlen und nominelle Lebensdauer. Berlin: Beuth Verlag, 2009
- [6] Aul, E.: Analyse von Relativbewegungen in Wälzlagersitzen. Doctoral thesis, TU Kaiserslautern, 2008
- [7] Maiwald, A.; Leidich, E.: Einflussfaktoren auf das tribologische Verhalten von biegefreien Wälzlagersitzen bei Relativbewegungen infolge Wandern. Aachen: Proceedings of the GfT Tribology-Meeting, Issue 51, 2010, pp. 31.1-31.19
- [8] Maiwald, A.: Numerische Analyse des Wanderverhaltens von Wälzlageringern. Doctoral thesis, TU Chemnitz, submitted 2013
- [9] Leidich, E.; Sauer, B.; Schiemann, T.; Thiele, S.: Definition und Auslegung von konstruktiven und tribologischen Abhilfemaßnahmen gegen tangentielle Wanderbewegungen von Wälzlageringern. Frankfurt/M.: Forschungsvereinigung Antriebstechnik e.V., Research project FVA 479 IV, 2012, running
- [10] Sonntag, R.: Über einige technisch wichtige Spannungszustände in ebenen Blechen. Habilitation dissertation, TH München, 1928